Marine Geology 463 (2023) 107120

Contents lists available at ScienceDirect

Marine Geology

journal homepage: www.elsevier.com/locate/margo

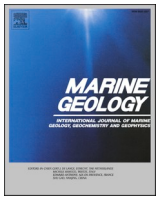

The impact of volcanic ash deposition and the Storegga Slide on organic carbon preservation processes in marine sediments near Iceland

Jana Blanke [a,b,*], Katharina Pahnke [a], Millie Bompard [c,d], Jack Longman [a,e,*]

[a] Marine Isotope Geochemistry, Institute for Chemistry and Biology of the Marine Environment (ICBM), University of Oldenburg, 26129 Oldenburg, Germany
[b] GEOMAR Helmholtz Centre for Ocean Research Kiel, D-24148 Kiel, Germany
[c] School of Ocean and Earth Sciences, National Oceanography Centre Southampton, University of Southampton, Southampton, UK
[d] Scottish Universities Environmental Research Centre, East Kilbride, UK
[e] Department of Geography and Environmental Sciences, Northumbria University, Newcastle-upon-Tyne, UK

ARTICLE INFO

Editor: Dr. Adina Paytan

Keywords:
Basaltic Tephra
Redox-conditions
Productivity
Turbidites
Reactive metal phases

ABSTRACT

The burial of organic carbon (OC) in marine sediments is a considerable sink for carbon, removing OC from the active ocean-atmosphere system. Both the total OC buried, and the proportion of OC retained in sediments after burial, varies by location, with some areas of the ocean floor known to be 'hotspots' of OC sequestration. Two potential such hotspots may be sediments containing high proportions of tephra (the unconsolidated products of explosive volcanism), and locations of turbidite deposition, but knowledge of specific burial regimes in such locations remains poorly constrained. To fully investigate these processes, we performed a holistic (organic and inorganic) geochemical analysis of samples from the Aegir Ridge, which contain both tephra layers and material from the Storegga Slide, a large turbidite. We show sediments found between the Storegga Slide and the tephra are a location of high OC preservation, linked to reducing conditions caused by the rapidly deposited slide layer sealing the sediments from overlying water column O_2. We see little evidence for tephra positively affecting OC preservation at our site, but this is likely a feature of specific burial conditions, with the responsible mechanisms depending highly on the nature of the tephra. Our findings demonstrate how even in locations proposed as OC burial hotpots, the processes controlling this burial are highly complex, and that levels of sedimentary OC burial must be assessed on a case-by-case basis.

1. Introduction

In the global carbon cycle, carbon is exchanged via fluxes between the atmosphere, biosphere, hydrosphere, geosphere and pedosphere (Falkowski et al., 2000). Some of the most important components of the global carbon cycle are processes which occur in the marine realm (Tanhua et al., 2013). Flux of carbon into the ocean currently absorbs as much as 25% of atmospheric CO_2, indicating its importance in the modern carbon cycle (Watson et al., 2020). One such process is termed the "biological pump", where photosynthesizing phytoplankton in the upper ocean converts the CO_2 to organic carbon (OC) during their life cycle (Cole et al., 2021; Falkowski et al., 1998).

When these organisms die, their remains sink out of the upper ocean. A proportion of this produced biomass is remineralized in the water column as the remains sink, and returns to the active marine carbon cycle, with the remainder reaching the underlying marine sediments (DeVries et al., 2012; Passow and Carlson, 2012). Upon reaching the sediment, some of this OC is buried, effectively sequestering the carbon in a stable form (Burdige, 2005; Cole et al., 2021). Consequently, the process of OC burial in marine sediments entails CO_2 removal from the atmosphere (Burdige, 2007; Falkowski et al., 2000), and may control carbon cycling on geological timescales. Between 30% and < 99% of the OC that reaches the seafloor is remineralized (Dunne et al., 2007; Henrichs, 1992), with the amount of OC buried relative to the amount remineralized termed 'burial efficiency'. This is generally dictated by the oxidation state of the sediment, with porewater O_2 availability leading to rapid aerobic microbial degradation of OC (Dunne et al., 2007; Hartnett et al., 1998).

One location proposed as a OC burial hotspot is marine sediment which regularly receives input of the products of explosive volcanism -

* Corresponding authors at: GEOMAR Helmholtz Centre for Ocean Research Kiel, D-24148 Kiel, Germany, and Department of Geography and Environmental Sciences, Northumbria University, Newcastle-Upon-Tyne, UK.
E-mail addresses: jblanke@geomar.de (J. Blanke), jack2.longman@northumbria.ac.uk (J. Longman).

https://doi.org/10.1016/j.margeo.2023.107120
Received 5 April 2023; Received in revised form 1 August 2023; Accepted 10 August 2023
Available online 11 August 2023

tephra (Longman et al., 2021). Tephra acts to enhance OC sequestration through a number of mechanisms (Longman et al., 2020; Longman et al., 2019). Immediately upon deposition in the ocean, the release of macro- and micronutrients (including P, N and Fe) from tephra can increase marine primary productivity by alleviating nutrient limitation in certain areas of the ocean (Longman et al., 2019; Moore et al., 2013). Examples of this process have been observed in the aftermath of numerous recent volcanic eruptions (Achterberg et al., 2013; Duggen et al., 2010; Olgun et al., 2011), this is also the case for many other deep-time volcanisms, e.g., the black shale was associated with numerous volcanic ash beds near the Ordovician-Silurian transition, and the end-Permian (Pohl et al., 2017). In addition to releasing large quantities of micronutrients to the upper ocean, tephra may also enhance burial efficiencies (Longman et al., 2019). Reactive metal phases (MeR), and in particular reactive iron (FeR) and manganese (MnR) are found in high quantities in tephra-rich sediments (Homoky et al., 2011; Longman et al., 2021; Longman et al., 2019). Reactive iron may act to protect OC and prevent microbial degradation through inner-sphere complexation, where Fe and OC form strong chemical bonds (Barber et al., 2017; Faust et al., 2021; Lalonde et al., 2012; Longman et al., 2022a; Longman et al., 2019), providing a protection mechanism which accounts for around 20% of all OC burial in marine sediments (Lalonde et al., 2012; Longman et al., 2022a). Additionally, MnR and reactive aluminum phases (AlR) are also associated with the preservation of OC (Homoky et al., 2011). Studies have shown the enhancement of OC preservation via AlR, by forming refractory organometallic complexes (Basile-Doelsch et al., 2007) and correlations between MnR and OC (Roy et al., 2013), likely a result of carboxylate groups bonding with Mn oxide surfaces (Johnson et al., 2015).

During diagenesis of tephra-rich sediment, the release of Fe(II) and Fe(III) can affect the redox environment in sediments (Costa et al., 2018; Crusius et al., 1996; Hembury et al., 2012; Maters et al., 2017). Fe(II) from tephra layers can cause the reduction of dissolved O_2 due to a double electron-cation transfer and the resulting oxidation of Fe(II)-silicate surfaces (Haeckel et al., 2001; Hembury et al., 2012). The extent of this solubility reaction depends on various factors, such as the oxidation state (as Fe(II) is more soluble than Fe(III)), mineralogy, crystallinity, structural impurities and the concentration and structure of organic ligands (Von der Heyden et al., 2012). These factors can be influenced by the process of eruption, as it affects the mineralogy and the oxidation state of Fe (Hoshyaripour et al., 2014). Indeed, the geochemical nature of the tephra, whether it is basaltic or andesitic, influences the ratio of Fe(II)/ Fe(III). In basaltic tephra, the Fe(II)/ Fe (III) is higher than in andesitic tephra, where the ratio is close to one (Horwell et al., 2007). In addition to the total amount of Fe(II) in tephra, the thickness of the tephra layer also influences the reduction of dissolved O_2. It has been shown, that a tephra layer of <1.5 cm can lead to a linear reduction of dissolved O_2 with depth (Hembury et al., 2012). The time intervals between tephra deposition are another factor influencing the rate of reduction. At intervals of ~150 years, the reduction rate will double, while with longer intervals the rate of the reduction will decrease (Hembury et al., 2012; Longman et al., 2019).

In addition to the deposition of tephra, it is possible that submarine landslides can also enhance OC preservation (Hage et al., 2022). Turbiditic and submarine fan facies are often high quality petroleum reservoir rocks, a result of their OC content (Meyers et al., 1996; Weimer and Link, 1991). This is typically because of their rapid burial, which acts to insulate OC from the oxidizing effect of overlying seawater (Huc et al., 2001; Meyers et al., 1996; Rullkötter et al., 1982). Examples of extremely OC rich sediment ($>$ 10 wt% OC) associated with turbidites have been observed in many areas of the seafloor environment, such as offshore western Africa (Biscara et al., 2011; Dean and Gardner, 1982), and Indonesia (Saller et al., 2006). Recent research has shown how turbidites may act to preserve young terrestrial OC, which is usually highly labile and is readily remobilized (Hage et al., 2020; Hussain et al., 2021). Further, it is also possible that large-scale turbidites such as the Storegga Slide act to transport nutrient-rich material to the open ocean, where limitations may otherwise exist, but this has yet to be clearly demonstrated. Located 70–150 km off the Norwegian West coast in the Norwegian Sea, with the deposition zone extending around 800 km NW and thus reaching the Aegir Ridge, the Storegga Slide occurred about 8200 years ago and is one of the biggest known landslides (Kvalstad et al., 2005). During the event, 2500 to 3500 km3 sediment was removed from the shelf (Bryn et al., 2005). Climatically, a period of century-scale global cooling (termed the 8.2 k event) took place around the same time as the emplacement of the Storegga Slide (Törnqvist et al., 2004). In the Northern Hemisphere surface temperatures dropped significantly (Aguiar et al., 2021; Barber et al., 1999; Hijma and Cohen, 2010).

In this work, we investigate the inorganic and organic geochemistry of a sediment core collected offshore Iceland. The sections studied contain both the Storegga Slide and a tephra layer, meaning the impact of both events on OC preservation and productivity can be investigated. We focused on the site's changes in redox and productivity history, as well as MeR contents caused by the Storegga Slide and the tephra layer and their combined impact on OC preservation processes. This study provides new insights into how two external sources of sedimentary material may impact the geochemistry of a deep-sea environment.

2. Materials and Methods

2.1. Study area

Core 88 was recovered on the 29th of July in 2014 near Iceland as part of the R/V Pelagia cruise 64PE391 from a water depth of 3670 m. Core 88 is 1311 cm long and contains varied sedimentary facies. The two most common are hemipelagic current sorted diamicton (HPD), which has a sandy clay texture and exhibits moderate to poor sorting, and mega turbidite deposits (MTD), which have an erosive base at the bottom and coarse, structureless sand with low mud content at the top. The Storegga Slide is one of these MTDs. (Watts, 2019). Sampling was completed on the Aegir Ridge, part of the Mid-Atlantic Ridge, in the far north of the Atlantic Ocean (Fig. 1) (Watts, 2019). The Aegir Ridge breaks up the Norway Basin in the Norwegian Sea, a marginal sea located northeast of Iceland adjacent to the North Sea, Barents Sea and the Greenland Sea (Mosar et al., 2002). The Norwegian Basin is bordered in the south by the Greenland-Scotland Ridge and in the north of the Jan Mayen Fracture Zone, which expands in the east to the Storegga slide source area (Brothers et al., 2013; Evans et al., 2005). Storegga is the continental slope located in the European North Sea, south of the Vøring-Plateau at the Norwegian coast (Hjelstuen et al., 2005). Additionally, variability of the North Atlantic Current, flowing along the Greenland-Scotland Ridge, influences the depositional environment of the Aegir Ridge (Hjelstuen and Andreassen, 2015).

The analyzed part of Core 88 from 17 to 220 cmbsf (centimeters below sea floor) is from between 1875 and 12,100 years before present (yr BP; (Watts, 2019) and comprises HPD and MTD (Fig. 2). Background sediments, which consist of HPD, were sampled at 17–30 cmbsf, 169–171 cmbsf and 179–220 cmbsf. The Storegga Slide (a MTD) occurs between 32 and 167 cmbsf, with one sample taken from this section at 75 cmbsf, although this is unlikely to represent the entire turbidite unit. With the use of terrestrial tsunami deposits, the Holocene Storegga Slide was dated to 8.17 cal ka BP (Bondevik et al., 2005; Dawson et al., 2011; Paull et al., 2010), while turbidite and offshore slide deposits in the Norwegian Basin dated it to 8100 $\pm$ 250 Cal BP (Haflidason et al., 2005).

The tephra layer sampled for this work occurs between 172 and 178 cmbsf (Fig. 2) and was geochemically matched to the Vedde eruption of 11,200 yr BP by comparison with a database developed by Watts (2019). Existing stratigraphic data and geochemical composition were used to match the tephra layer to the most plausible eruption match (Watts, 2019).

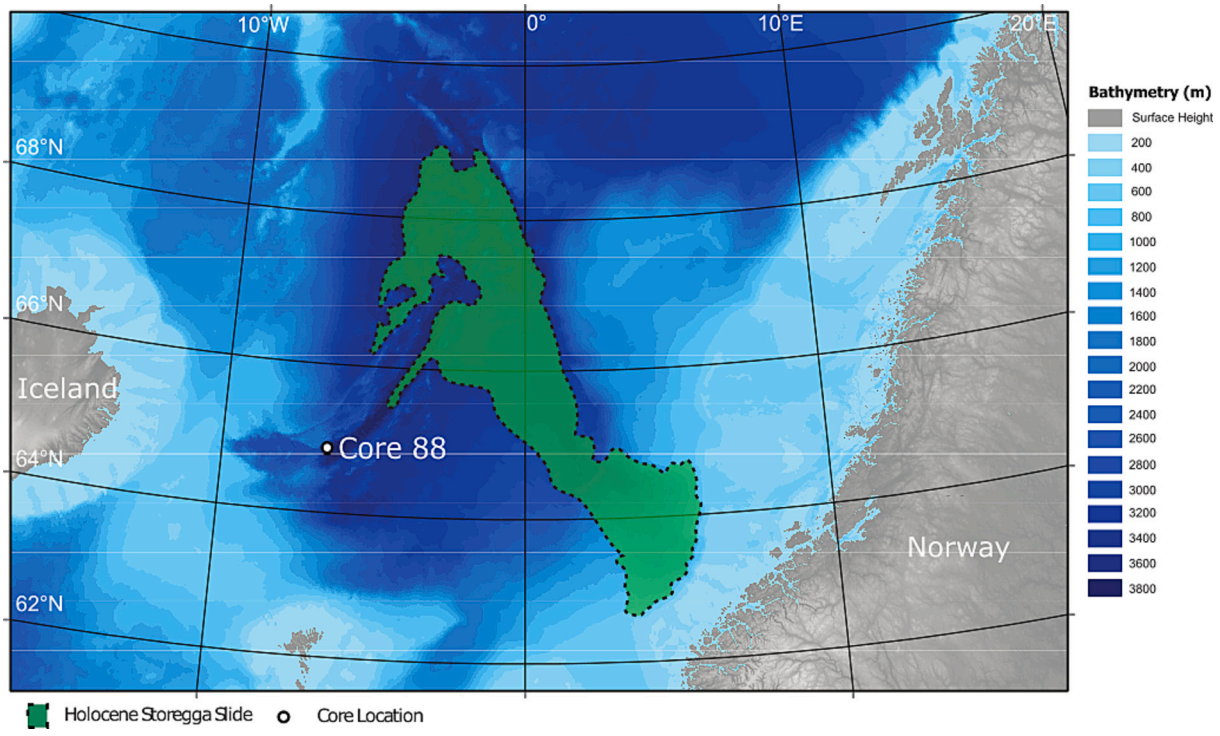

Fig. 1. Location of drilling site of Core 88, drilled by the RV Pelagia, as part of cruise 64PE391, in the Norwegian Sea. Also indicated on the map is the estimated extent of the Holocene Storegga slide (adapted from Watts, 2019). Location of core is outside of mapped Storegga debrite bed, but Storegga-related material was identified via geochemical analysis, see Watts (2019).

2.2. Geochemical analysis

2.2.1. Extraction of trace metals and main elements

All sediment samples were freeze dried and homogenized prior to total digestion. Roughly 50 mg dry weight of each sample were weighed before 1 mL of concentrated HNO_3 was added to dissolve most base element sulfides and sulfates. Subsequent additions of concentrated HF (2.5 mL) and $HClO_4$ (0.5 mL) were completed prior to reflux and followed by evaporation to ensure complete digestion of all silicates. Upon reaching dryness, 3 mL of 6 M HCl were added to the samples and evaporated to ensure the dissolution of all carbonates and the complete evaporation of HF. After this, 0.5 mL of conc. HNO_3 were added and made up to 25 mL with MilliQ ultra-pure water, as a preservative for the samples. All acids were of ultrapure quality. Certified reference materials (CRMs; HISS-1 marine sediment and BHVO-2 basalt) and method blanks were prepared in the same manner.

Trace metal contents were analyzed via mass spectrometric methods at the Institute for Chemistry and Biology of the Marine Environment (ICBM), Oldenburg. Vanadium (V), molybdenum (Mo), uranium (U) and zinc (Zn) were analyzed to be used as redox-proxies, whereas manganese (Mn) and iron (Fe) were analyzed to support the analysis of their corresponding reactive metal phases. Samples from 30 to 180 cmbsf were diluted and analyzed on a Thermo Fisher Element 2 inductively coupled plasma mass spectrometer (ICP-MS). Due to instrumental issues, samples from 20 to 29 cmbsf and 181–210 cmbsf were analyzed with a Thermo Fisher iCAP PRO inductively coupled plasma optical emission spectrometer (ICP-OES). Calibration for both methods was carried out by measuring synthetic standards with quality control performed by measuring in-house standards and CRMs. Repeat measurements of CRMs indicate the reliability of the digestion and analysis, with concentrations of most elements used in this study within 10% of expected values, except V in the HISS-I Standard in the first total digestion with precision RSD of 13.06% (Supplementary Table S1–3). Blank concentrations were negligible.

To enable comparison between samples with different mineralogy, the trace metal content was normalized to Al content (Calvert and Pedersen, 1993). In addition, enrichment factors (EFs) were also calculated using Al as the normalizing element and the composition of post Archaean Australian shale (PAAS) (McLennan et al., 1983) representing average continental crust compositions according to eq. 1.

$$Me_{EF} = \frac{\left(\frac{Me}{Al}\right)_{sample}}{\left(\frac{Me}{Al}\right)_{shale}} \quad (1)$$

Where Me is the trace metal of interest. If EF of an element is >1, the element is enriched. If EF of an element is <1, it is depleted relative to PAAS (Algeo and Li, 2020; Tribovillard et al., 2006). To determine the amount of barium derived from productivity as an indicator of paleoproduction, the amount of biogenic barium (Ba_{Bio}) was calculated using eq. 2 (Schoepfer et al., 2015):

$$Ba_{Bio} = Ba_{Total} - Al_{Total} * \left(\frac{Ba}{Al}\right)_{detrital} \quad (2)$$

The ratio of (Ba/Al) from PAAS was used as $(Ba/Al)_{detrital}$ (McLennan et al., 1983). Studies have shown that the calculated concentration of Ba_{Bio} strongly depends on the chosen $(Ba/Al)_{detrital}$ value (Cai et al., 2010), and that data from the detrital fraction of the analyzed sediments is preferable for the calculation of Ba_{Bio}. However, due to a lack of detritus-dominated samples, this was not possible for this study. To ensure consistency, the Ba/Al ratio of PAAS was used instead, as PAAS was used for all EF calculations.

2.2.2. Extraction of reactive iron and manganese

To determine the concentration of iron- and manganese-oxyhydroxides, the sediments underwent a dithionite extraction (Faust et al., 2021; Kostka and Luther III, 1994; Mehra and Jackson, 2013). Roughly 100 mg of each sample were weighed into a 30 mL centrifuge tube. 15 mL of a solution containing 0.27 M trisodium citrate ($Na_3C_6H_5O_7{*}H_2O$) and 0.1 M sodium bicarbonate ($NaHCO_3$) were added to the samples and heated to 80 °C in a water bath. To this mixture, 0.1

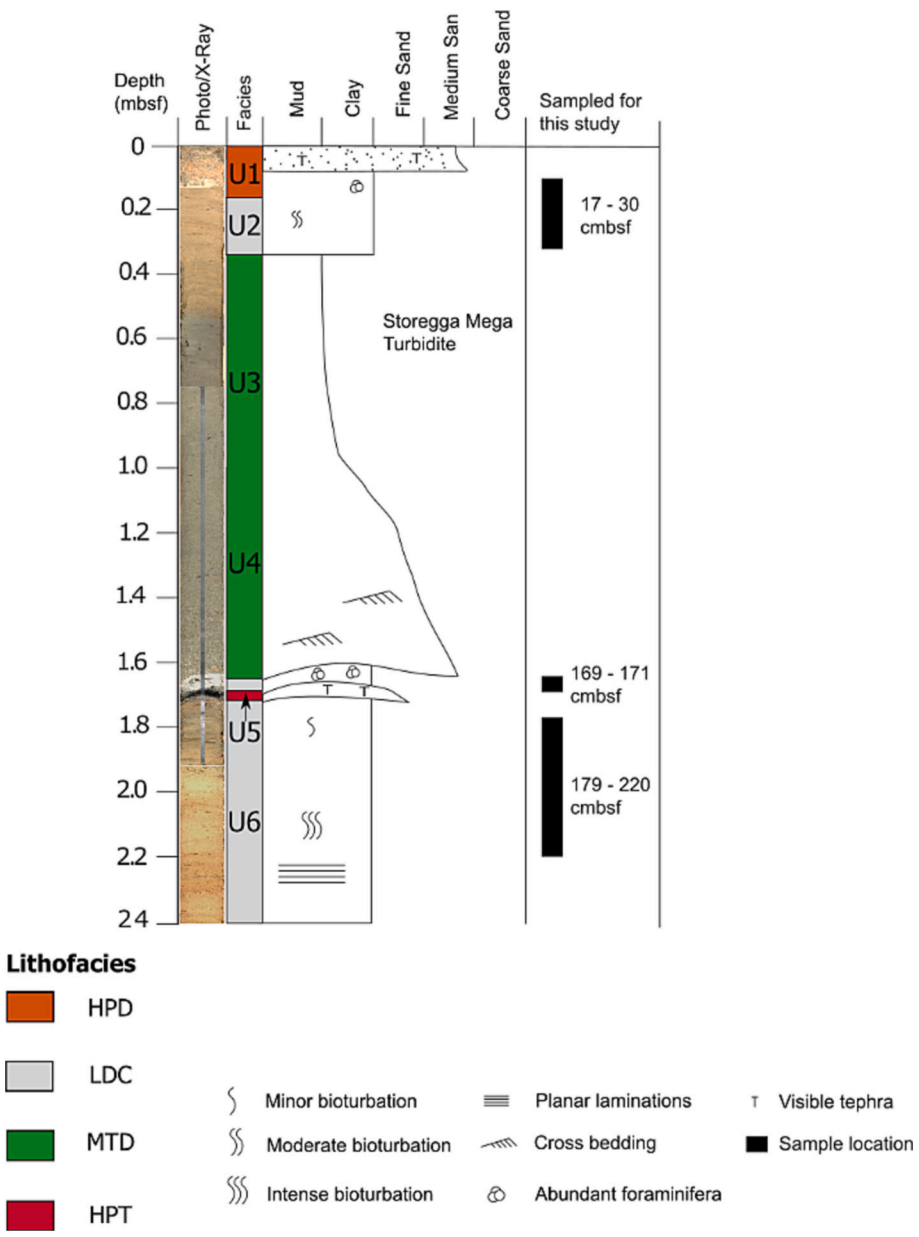

Fig. 2. Lithological log of core 88, indicating the location of the key horizons studied here (highlighted with black rectangles). Facies abbreviations are taken from Watts (2019): HPD (Hemipelagic current sorted diamicton), LDC (Lag deposit contourite), HPT (Visible tephra horizon - hemipelagic and tephra) and MTD (mega turbidite deposit). The location of the Storegga slide is unit 3 (U3), with the Vedde tephra unit 5 (U5). X-Ray micrograph and photos collected using British Ocean Sediment Core Repository (BOSCORF) ITRAX scanner.

M sodium dithionite ($Na_2S_2O_4$) was added, with temperature maintained for 15 min, during which samples were mixed three times. Subsequently, the mixture was centrifuged and the supernatant was decanted. To prevent precipitation of Fe(III) prior to analysis, 200 μL of conc. HCl was added to the supernatant.

Concurrently, a control leaching was conducted to assess MeR extraction by seawater. About 100 mg of five samples and one standard (HISS-I) were subjected to a leaching process similar to the reduction process described above. Here, the complexing and reducing agents were replaced by sodium chloride (NaCl), to obtain a solution with the same ionic strength (Faust et al., 2021; Kostka and Luther III, 1994; Lalonde et al., 2012; Mehra and Jackson, 2013). All samples were diluted with 2% HNO_3 for analysis on a Thermo Fisher iCAP PRO ICP-OES at the ICBM. As with the total digests, synthetic standards were used to develop a calibration curve, with quality control completed via in-house standards (Supplementary Table S4).

2.2.3. Organic carbon

Organic carbon content was measured using an Elementar Vario PYRO Analyser (EA) at the British Geological Survey. Samples were first exposed to 10% HCl until all carbon had dissolved, and then washed multiple times with Milli-Q water prior to analysis. For further information we refer the reader to Watts (2019).

2.2.4. Validation of PAAS as reference material

As we are reliant on enrichment factors to assess redox state in our sediments, we must determine which reference material is suitable for this. To investigate the suitability of PAAS as reference material for this study, we calculated trace metal EFs and Ba_{Bio} concentrations relative to the basaltic reference material Japanese Basalt 3 (JB-3) (Govindaraju, 1994), and compare the results to those calculated with PAAS.

Fig. 3 indicates how V_{EFs}, Fe_{EFs} and Mn_{EFs}, are lower when calculated using JB-3, but the general pattern is the same as EFs calculated relative to PAAS. Apart from two samples from the topmost section at 21 and 25 cmbsf, JB-3 Mo_{EFs} display values >2 in the same samples as PAAS Mo_{EFs}. Both reference materials show Mo_{EFs} in the same range. U_{EFs} and Zn_{EFs} calculated with JB-3 show higher values (Fig. 3), but this does not impact our interpretation.

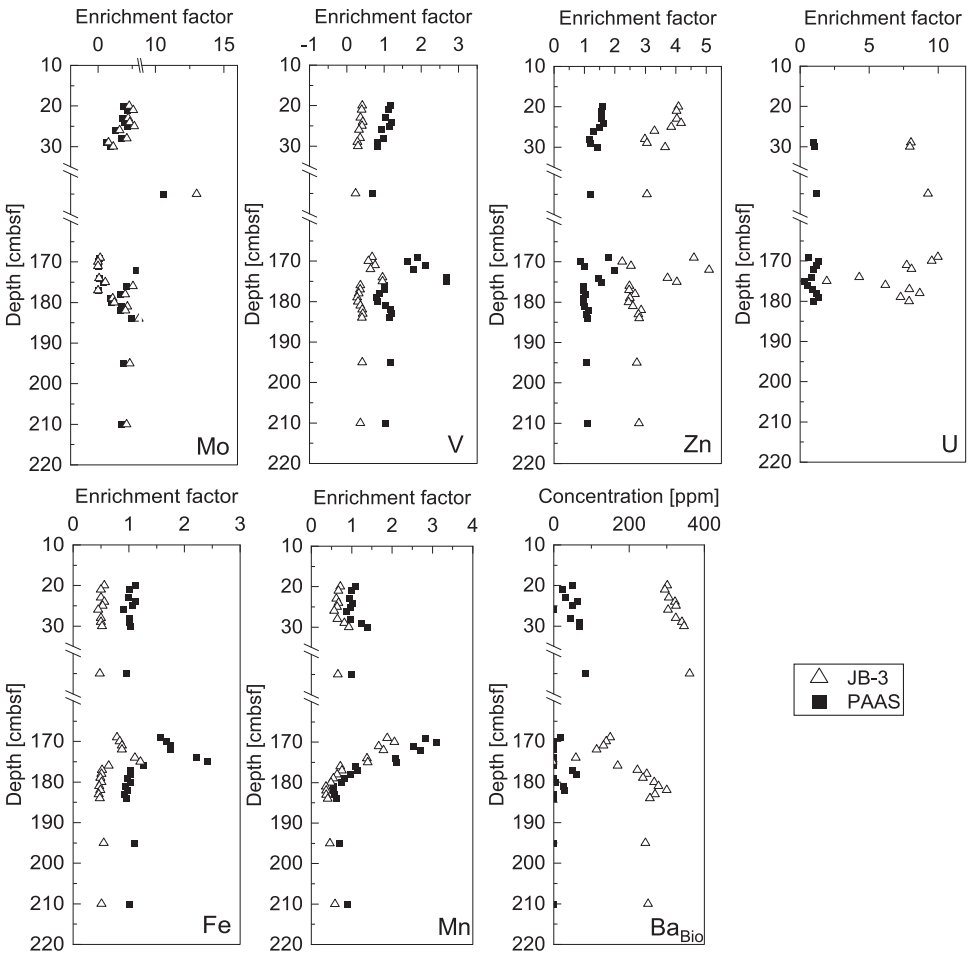

Fig. 3. Depth profiles of the enrichment factors of Mo, V, U, Zn, Mn and Fe and the concentration of Ba_{Bio} [ppm] calculated with PAAS and JB-3.

Ba_{Bio} concentration calculated with JB-3 show higher values than concentrations calculated with PAAS. However, JB-3 Ba_{Bio} and PAAS Ba_{Bio} values show a strong correlation ($r = 0.88$; $p = 0.000$), as do PAAS Ba_{Bio} values with other reference materials JA-1 ($r = 0.93$; p = 0.000) and BHVO-2 ($r = 0.83$; p = 0.000) calculated Ba_{Bio} values (Govindaraju, 1994; Jochum et al., 2016; McLennan et al., 1983). Thus, we interpret positive Ba_{Bio} concentrations as non-detrital Ba. Due to the close comparison between PAAS and JB-3, we conclude PAAS is a suitable reference material for the data analyzed in this paper. All calculated EFs are found in the supplementary, where also include data normalized to two further reference materials (JA-1 and BHVO-2), further demonstrating how changing the normalizing reference does not alter our conclusions (Supplementary Table S10–12).

3. Results

3.1. Vanadium and molybdenum

Downcore values of vanadium enrichment factors (V_{EF}) vary between 0.68 and 2.67, with an average of 1.25. The highest value occurs in the tephra layer (between 172 and 177 cmbsf), while the lowest value is found in the Storegga Slide sample (75 cmbsf) (Fig. 4). Molybdenum concentrations are all <2 ppm, except in the Storegga Slide sample (9.09 ppm). This provides the only notable Mo_{EF} of 10.59, while all other Mo_{EFs} are <2, thus not significant (Fig. 4).

3.2. Uranium and zinc

Uranium enrichment factors (U_{EF}) are only available for the samples between 30 and 180 cmbsf, as U could only be accurately measured on the ICP-MS, which was not available to measure the other samples as they belonged to a later digestion batch. As all U concentrations are <3 ppm, U has been deemed not suitable as a redox-proxy in this work (Fig. 3).

Zn shows an average enrichment factor (Zn_{EF}) of 1.26. Values <1 can be found in six samples throughout the section with values between 0.87 and 0.98 at 170–170 cmbsf, 179–180 cmbsf and at 176–177 cmbsf. All other samples show $Zn_{EFs} > 1$ with the highest value of 1.98 in the tephra layer at 172 cmbsf (Fig. 4).

3.3. Manganese, iron, reactive Mn and reactive Fe

Manganese enrichment factor (Mn_{EF}) downcore values vary between 0.54 and 3.11 with an average of 1.27. The sediments at 169–171 cmbsf display the highest values, while the bottom sediments at 181–210 cmbsf show the lowest values (Fig. 5).

MnR concentrations vary between 0.003 and 0.042 wt% with an average of 0.023 wt%. Throughout the core, the concentrations fluctuate strongly. While the sediments at 17–30 cmbsf and 169 cmbsf display relatively stable concentrations around 0.030–0.042 wt%, concentrations at 179–220 cmbsf fluctuate between 0.003 and 0.037 wt%. The Storegga Slide and the tephra layers display mostly low values around 0.005–0.016 wt% (Fig. 5).

Iron enrichment factors (Fe_{EF}) range between 0.81 and 2.41 with an average of 1.20. Highest Fe_{EF} values (1.57–2.41) can be found in the tephra layer and in the sediments at 169–171 cmbsf, while the other samples show values around 0.81–1.11. (Fig. 5).

The concentrations of FeR range between 0.11 and 0.85 wt% with an

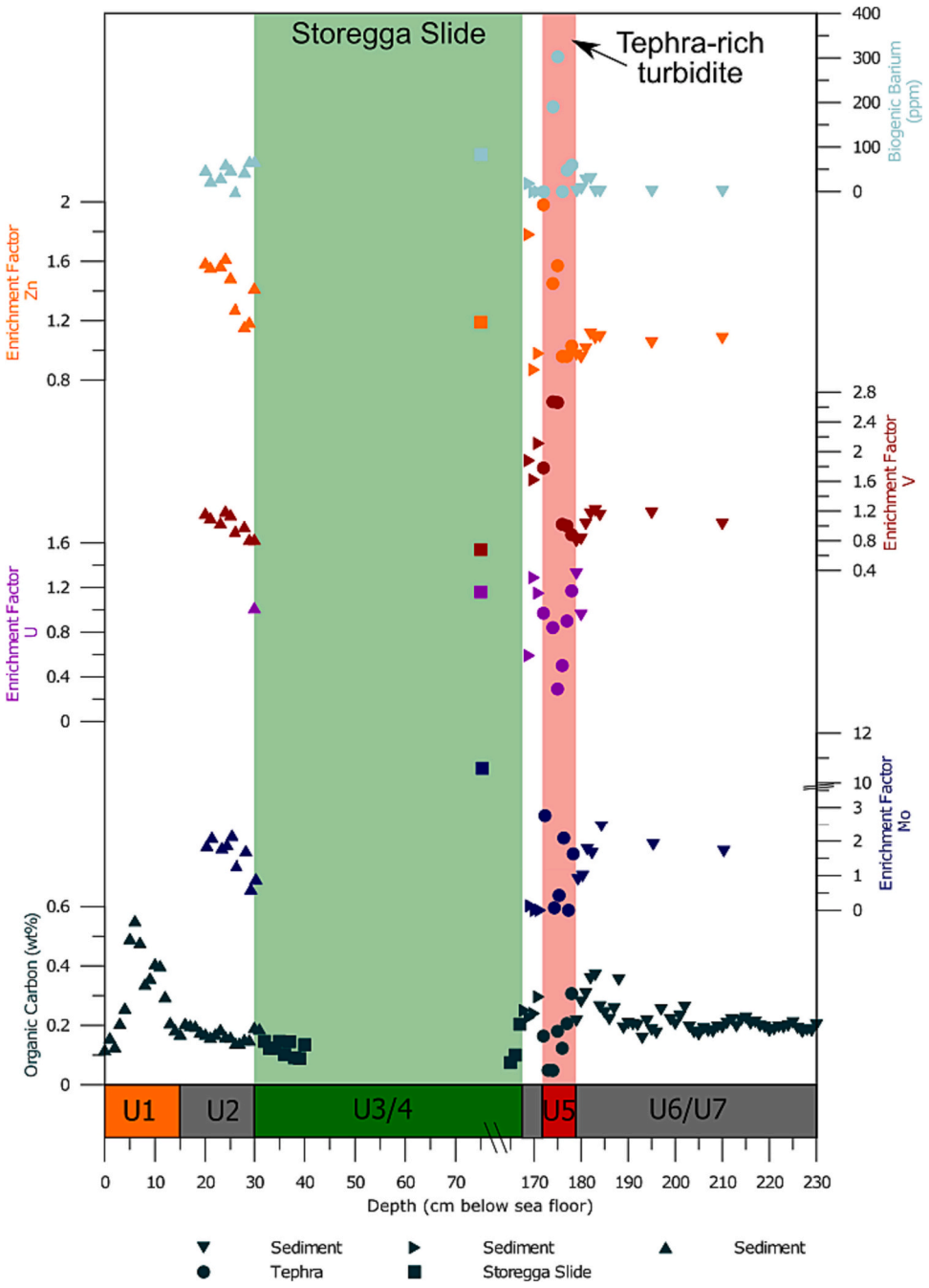

Fig. 4. Depth profiles of the organic carbon content [wt%] (Watts, 2019), the enrichment factors of Mo, V, U and Zn, and the concentration of Ba_{Bio} [ppm]. Lithofacies and unit numbers are as in Fig. 2. Also highlighted are the locations of the Storegga Slide (green rectangle) and the tephra-rich turbidite (red rectangle). (For interpretation of the references to colour in this figure legend, the reader is referred to the web version of this article.)

average of 0.49 wt%. The lowest concentrations can be found in the tephra layer, while the sediments at 195–220 cmbsf show the highest concentrations (0.70–0.85 wt%). Sediments at 17–30 cmbsf display a relatively stable downcore distribution with most of the concentrations varying around 0.52–0.69 wt%. (Fig. 5).

3.4. Biogenic barium

Ba_{Bio} is found throughout the core with concentrations varying between 0.17 and 83.18 ppm. The highest concentrations can be found in the Storegga Slide (83.18 ppm) and in the topmost sediments at 17–30 cmbsf. Only the sediment samples at 170–171, 179 and 183–210 cmbsf and the tephra sample at 172–176 cmbsf show no Ba_{Bio} (Fig. 4).

3.5. Organic carbon

Organic carbon concentrations range between 0.05 and 0.37 wt% with an average of 0.21 wt%. The bottom sediments at 179–210 cmbsf display the highest average concentration (0.27 wt%), while topmost sediments show the lowest average concentration (0.16 wt%). The tephra layer displays the highest fluctuation with concentrations ranging between 0.05 and 0.31 wt% and an average of 0.17 wt%. The OC concentrations in the sediments at 169–171 cmbsf average at 0.25 wt % (Fig. 4).

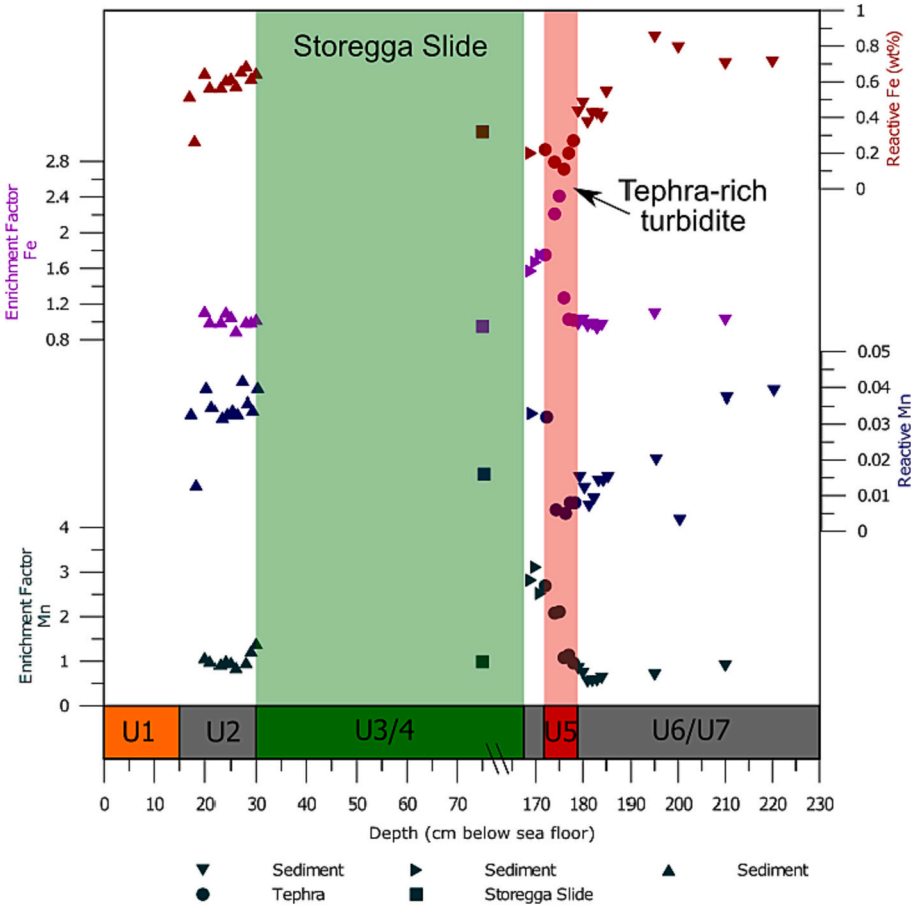

Fig. 5. Depth profiles of the enrichment factors of Mn and Fe and of the concentrations of FeR and MnR [wt%]. Lithofacies and unit numbers are as in Fig. 2. Also highlighted are the locations of the Storegga Slide (green rectangle) and the tephra-rich turbidite (red rectangle). (For interpretation of the references to colour in this figure legend, the reader is referred to the web version of this article.)

4. Discussion

4.1. Changing oxidation state and reactive metal phases

To investigate the changing redox history of the site, we use a range of trace metal concentrations and enrichment factors. Following the approach of Algeo and Li (2020), we use the enrichment of Mo and V as indicators of oxygen depleted/sulfidic conditions in the sediment column.

Vanadium starts to accumulate in sediments under suboxic-anoxic conditions as the solubility of V is lowered after the reduction of V (V) to V (IV) and is further reduced to V (III) under sulfate reducing (euxinic) conditions (Breit and Wanty, 1991; Morford and Emerson, 1999; Tribovillard et al., 2006). Molybdenum is only enriched under euxinic (Adelson et al., 2001; Brumsack, 1989; Calvert and Pedersen, 1993; Huerta-Diaz and Morse, 1992). Conversely, depletion is indicative of oxic conditions under which Mo is most commonly found in seawater as molybdate (MoO_4^{2-}), a stable and largely unreactive Mo (VI) species (Morford et al., 2009).

Mo enrichment can only be seen in the Storegga Slide sample. With a concentration of 9.27 ppm and thus a Mo_{EF} of 10.59, this hints at hints at oxygen deficient conditions, maybe even sulfidic in parts of this sample (Algeo and Li, 2020; Brumsack, 1989). However, the Storegga Slide is a mix of long-distance mud, whereas the remainder of the core consists of sediment deposited in situ. Therefore, the high Mo_{EF} may not be indicative of depositional oxidation state, rather the conditions in the shelf sediment comprising the Storegga Slide. There is no evidence of redox-related enrichment in all sediment and tephra samples, as Mo concentrations <2 ppm represent crustal values (Fig. 4). Furthermore, V only displays $V_{EFs} > 2$ in three samples. One sediment sample at 171 cmbsf and two tephra samples at 174–175 cmbsf, hinting at oxygen-depleted condition in these samples. All other samples display $V_{EFs} < 2$, showing neither enrichment nor depletion.

Zn enrichment would indicate sulfidic and low oxygen sediments, as Zn enrichment is shown to represent reducing conditions with high sulfate availability (Costa et al., 2018; Huerta-Diaz and Morse, 1992). However, while mild Zn enrichment would hint a trend towards low-oxygen conditions, Zn_{EFs} are still below a threshold of 2, which means that they cannot be deemed significant. All samples show neither enrichment nor depletion, where depletion would indicate more oxidizing conditions (Costa et al., 2018).

Mn enrichment indicates oxic conditions, while depletion is indicative of suboxic to anoxic conditions (Aller, 1994; Froelich et al., 1979; Scholz et al., 2011). However, use of Mn as a proxy for oxidation state is uncertain. Calvert and Pedersen (1993) declared Mn as a subpar redox proxy, as measurements of Mn fluxes in the eastern Pacific showed insufficiently high Mn concentrations during an oxygen minimum (Johnson et al., 1992). Tribovillard et al. (2006), came to the same conclusion, as Mn is very mobile during reducing conditions and could either be trapped as oxides or authigenic Mn-carbonates or released to the water column, so we interpret the data presented here with caution. As Mn, Fe enrichment occurs under oxic conditions, as Fe (II) oxidizes to Fe (III) and precipitates as Fe oxyhydroxides (Homoky et al., 2011; Little et al., 2015; Maters et al., 2017). Fe (II) is less soluble than Mn (II) and can form insoluble forms such as Fe (II)-carbonate ($FeCO_3$) and sulfides like pyrite (FeS_2) (Burdige, 1993). Therefore, Fe should also only be used

to a limited extent in order to estimate redox-conditions.

Samples in the core-parts at 17–30 cmbsf and 179–210 cmbsf show no indication of depletion or enrichment (Mn_{EFs} between 0.86 and 1.40). This in combination with the behavior of the other trace metals indicates most likely oxic conditions in these core-parts. Only the sediments below the Storegga Slide and the top of the tephra layer display $Mn_{EFs} > 2$, with the sediments showing stronger enrichment with values of 2.52–3.11 hint at suboxic conditions (Fig. 5). The enrichment of both Mn and Fe in the sediments below the Storegga Slide was probably caused by the sudden influx of sediment, as it may have reduced the ability of seawater oxygen to percolate into the sediments below, thus promoting low oxygen conditions(Crusius and Thomson, 2000; Thomson et al., 1993; Thomson et al., 1998).

The low concentrations of Mn, Fe and their respective reactive metal phases in the source sediment from the Storegga suggest a low concentration of both trace metals since the beginning (Watts, 2019), rather than the impact of changing redox-conditions (Fig. 5). Moreover, the tephra does not appear to supply MnR, as overall MnR concentrations in the tephra layer are low.

Additionally, the studied tephra layer shows the highest Fe_{EFs} (1.02–2.41), but with comparatively low FeR concentrations (0.11–0.22 wt%) (Fig. 5). Contrary, Fe_{EFs} in the sediment sections (17–30, 169–171 and 179–210 cmbsf) show neither enrichment nor depletion, while showing far higher FeR concentrations than the tephra. The top sediments show concentrations of 0.52–0.69%, while the bottom sediments show concentrations up to 0.85%. This also indicates that the tephra did not act as a source of FeR to sediments in its vicinity. This could be due to the basaltic nature of the tephra (Watts, 2019), since research which showed high FeR (and therefore high oxidizing potential) in tephra was based on andesitic tephra (Hembury et al., 2012; Homoky et al., 2011). The nature of the tephra in this core also may explain why the sediments below the Storegga Slide show the lowest FeR concentrations (0.20 wt %) (Fig. 5). While studies have shown higher OC bound to FeR in sediments surrounding tephra layers, than other sediments (Homoky et al., 2011; Longman et al., 2021), thus indicating tephra as a source for MeR, this did not seem to be the case in this core due to the basaltic nature of the tephra (Watts, 2019). Additionally, the tephra is contained in a turbiditic flow deposit, and so it is possible that the transport process has led to the release of reactive metal phases.

The MnR shows a similar pattern as FeR except for low concentrations in the sediment under the tephra layer (0.017 wt%) and high concentration in the sediments below the Storegga Slide (0.033 wt%) (Fig. 5). The bottom sediments also hint Mn depletion, with the lowest Mn_{EFs} of all samples. With values between 0.54 and 0.89, these samples show a far stronger depletion, than any samples of the topmost section (Fig. 5). This indicates, that MnR concentrations may have an added impact on Mn concentrations next to the oxic conditions in this core-part. Overall, the data suggests oxic conditions in the top and bottom sediments and oxygen depleted (most likely suboxic conditions) in the tephra and the sediments below the Storegga Slide. Furthermore, accumulation of Mo, V and Zn in the sediments is suggested to be influenced by organic matter types, thus the limited use in this study. While enrichment factors are preferable to bimetal proxies, a consistent redox-pattern requires the extended use of inter-elemental relationships of multiple redox-proxies (Algeo and Liu, 2020). This approach should be used for future studies on the influence of the turbidite and tephra on redox conditions of Core 88 and other locations.

4.2. Paleo-productivity

In marine sediments, most Ba is sourced from the water column, where it occurs as barite ($BaSO_4$). Delivery is primarily from barite bound to decaying and sinking OM. Therefore, barite fluxes are mostly correlated to OM fluxes and a Ba enrichment in the sediments is seen as an indicator for paleo-productivity (Fig. 4) (Schoepfer et al., 2015; Tribovillard et al., 2006). However, Ba also adsorbs to various sedimentary phases unrelated to productivity (Dymond et al., 1992), we therefore interpret only the Ba fraction correlated to OM fluxes (Ba_{Bio}, or the biogenic barium component, see Materials and Methods). Moreover, the Ba_{Bio} concentration of a sample is put in perspective to the other samples of the core-part and clearly distinguishable positive values interpreted accordingly as higher or lower productivity.

The highest Ba_{Bio} concentration of all analyzed samples is found in the Storegga Slide (Fig. 4), but as this is turbiditic comprised of long-distance transported shelf sediment (Fig. 1), it may simply be an indication of high productivity on the shelf at some point in the Quaternary (when the shelf sediments first deposited). Above the Storegga Slide, all samples show elevated Ba_{Bio} (Fig. 4), indicating increased paleo-productivity relative to the remainder of the core. It must be noted however, that this perceived rise in productivity is potentially a feature of the composition of samples prior to the Storegga slide, rather than an absolute increase in productivity. The Storegga Slide may have played a supporting role in enhancing the paleo-productivity shortly after deposition, due to the ability of turbidites to transport material (and therefore also nutrients) off the continental shelf into open ocean locations. This would have promoted short-term productivity in a nutrient limited region (Pierau et al., 2011; Shanmugam, 2002), though the current dataset cannot definitely confirm this. Moreover, sudden nutrient supply, does not support long-term enhancement of productivity regimes. Changes in the boundary conditions, such as flooded shelves and modified ocean currents are more likely to be the cause for the long-term enhancement of productivity (Haflidason et al., 2005; Smith et al., 2004; Smith et al., 2015).

4.3. Impact of shifting sedimentary regimes on OC preservation

With a concentration range of 0.2–0.4 wt%, the core shows limited variability, like the proxies for redox-conditions. Nevertheless, deviations from the average OC concentration of the three sediment sections (0.21 wt%) of the whole core-part and average OC concentrations of the different sections were used to see if a pattern can be discerned in relation to the other proxies.

The uppermost sediment section (17–30 cmbsf) displays indication of increased paleo-productivity in all samples, while EFs indicate oxic conditions (Fig. 4). FeR and MnR concentrations are also relatively high compared to other sections of sediment (Fig. 5), but despite mostly positive indicators for an increased OC preservation (Barber et al., 2017; Burdige, 2007; Faust et al., 2021; Longman et al., 2021), the section shows the lowest average OC concentrations of all sediment samples (0.17 wt%) (Fig. 4). This suggests in this environment, production rather than preservation is the controlling factor dictating OC burial rates (Lu et al., 2019). Alternatively, the data may imply that other factors like sedimentation rate, climatic changes and changing sediment composition may have had a strong impact on OC preservation, acting to enhance remineralization, thus counteracting favorable OC preservation conditions. However, the existing dataset lacks sufficient information to exclude or include certain factors, with further research on Core 88 necessary.

EFs in the Storegga Slide (75 cmbsf) sample indicate the presence of reducing conditions (Adelson et al., 2001; Calvert and Pedersen, 1993; Huerta-Diaz and Morse, 1992; Schoepfer et al., 2015), increased paleo-productivity (Fig. 6) and lower FeR and MnR concentrations than most sediment samples (Fig. 5). However, as in the uppermost sediments, these indicators for favorable OC preservation did not lead to high OC content, with the Storegga Slide containing lowest average OC concentrations of all sections (0.12 wt%) (Figs. 4, 6). This could stem from low OC concentrations in the source sediment to begin with, from the low MeR concentrations in this section or a combination of these two. Even if redox conditions (i.e. low oxygen) may have been favorable for preservation (Burdige, 1993), low MeR concentrations would take away an important preservation mechanism (Longman et al., 2021) for the existing OC in the sediments, resulting in low OC concentrations in the

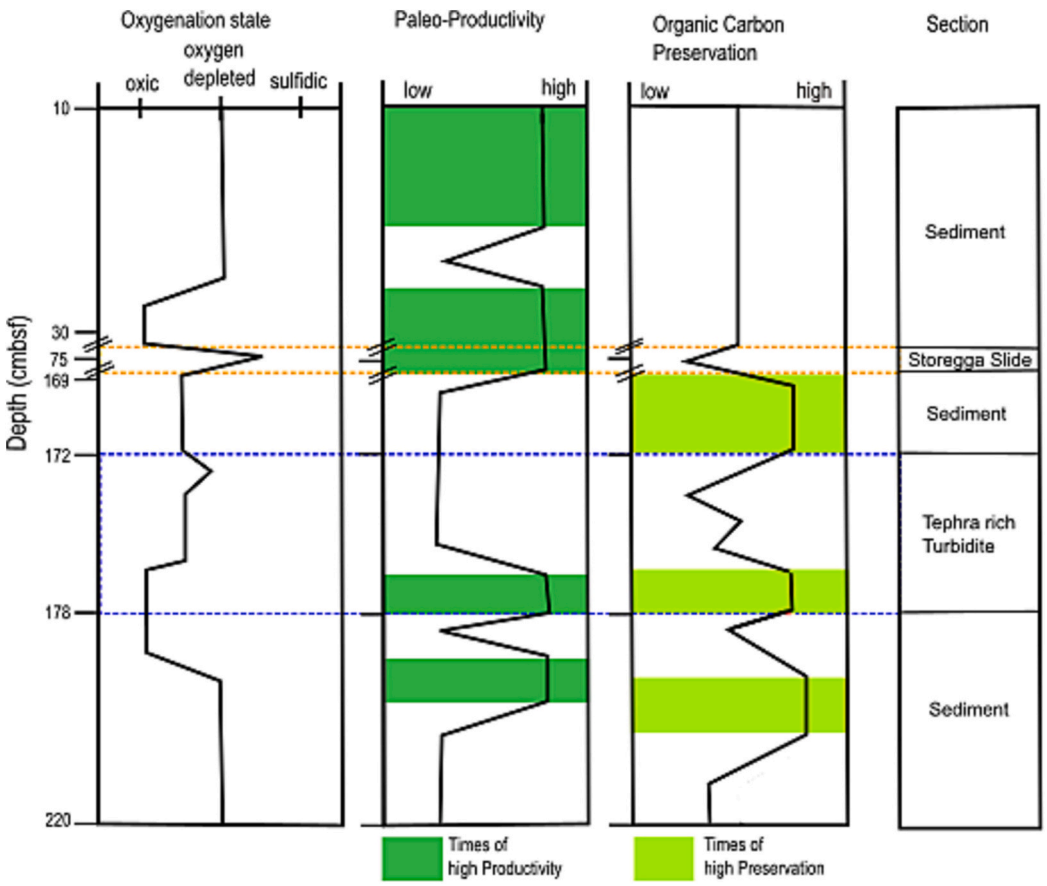

Fig. 6. Schematic representation of the oxygenation state, degree of paleo-productivity and degree of organic carbon preservation within the analyzed sections of the core-part. Oxygenation state was derived from enrichment factors of Mo, V, U and Zn, paleo-productivity was derived from the Ba_{Bio} concentrations and organic carbon preservation from C_{org} concentrations.

samples. Moreover, since there is only one turbidite sample, there may be significant variation in the slide facies that our resolution cannot account for. The Storegga Slide consists primarily of unstructured coarse sand with low mud content devolving into medium sands (Watts, 2019), which is not resolved in our resolution. Thus, interpreted conditions only apply to this specific sample.

Sediments directly below the Storegga Slide (169–171 cmbsf), show an average OC concentration of 0.25 wt%, higher than the core-part average (0.21 wt%; Fig. 4). Geochemical proxies hint at oxygen depleted, most likely suboxic, conditions (Anderson, 1982; Crusius et al., 1996; Morford and Emerson, 1999), with no indication of paleo-productivity compared to the other sediment sections (Fig. 6) (Schoepfer et al., 2015). As such, OC content in this section appears to be controlled by reduced oxidant exposure due to the oxygen deficient conditions (Fig. 6) In addition, high MnR content suggests complexation between OC-MnR may also be a valuable pathway for preservation (Homoky et al., 2011; Johnson et al., 2015). Such a finding has only been proven in laboratory experiments, where birnessite (the most common Mn-oxide) was found to form bonds with carboxylate groups of OC particles (Johnson et al., 2015). The unique sedimentation regime of the section may be the cause of such low oxygen and associated high preservation. This section is found below the Storegga Slide, and above the tephra layer. The sudden influx of sediment may have reduced the ability of seawater oxygen to percolate into the sediments below, thus promoting low oxygen conditions (Crusius and Thomson, 2000; Hartnett et al., 1998; Thomson et al., 1993; Thomson et al., 1998).

The tephra layer (172–180 cmbsf) exhibits the lowest FeR and MnR concentration of all analyzed samples (Fig. 5), indicating that it is not a source of MeR to the overlying layer. This supports the suggestion that low oxygen caused by the Storegga Slide may be the primary reason for above core-part average OC content.

Moreover, the tephra samples indicate oxygen depleted conditions, suggested by the enrichment factors of Mn and Fe (Fig. 4). Additionally, the tephra shows elevated Ba_{Bio} concentrations in the two bottom samples (Fig. 6) (Schoepfer et al., 2015) and very low average OC concentrations (0.15 wt%) in comparison to the sediments surrounding the tephra (0.25 wt% and 0.22 wt%). The two bottom samples also show the highest OC concentrations (0.21 and 0.31 wt%) of the tephra. It must be noted that the Vedde tephra was 11,200 yr BP, around the onset of the Holocene. Thus, this rise in productivity may also be linked to the warming at the end of the glacial period (Osman et al., 2021), rather than nutrient supply by the tephra (Browning et al., 2015; Longman et al., 2022a; Longman et al., 2019). Further studies of the Vedde tephra across a wide range of locations would be necessary to assess the possibility of Vedde tephra causing productivity.

In addition, with an average of 0.21%, higher OC concentrations are concentrated in the top samples of the bottom sediment section, same as positive Ba_{Bio} concentrations (180–183 cmbsf). This could imply increase in OC concentration due to elevated production, as the present oxic conditions would not have been favorable for OC preservation.

A comparison of our data with the literature revealed results that were similar, such as turbidites enhancing OC preservation by isolating OC from overlying seawater via rapid burial. (Huc et al., 2001; Meyers et al., 1996; Rullkötter et al., 1982). This was demonstrated in the analyzed part of Core 88, where the Storegga Slide seems to have enhanced OC burial in the sediments below, though rapid burial.

But our data also showed results in regards to the tephra, that differed from former studies. Literature revealed stimulated upper ocean

productivity via the release of macro-and micronutrients after deposition (Achterberg et al., 2013), as well as enhanced burial efficiencies via reactive metal complexation. Here, the tephra showed high amounts of FeR and MnR, which protected OC and prevented microbial degradation via inner-sphere complexation (Barber et al., 2017; Faust et al., 2021; Lalonde et al., 2012; Longman et al., 2019; Longman et al., 2022b). Our data showed that the tephra from Core 88 had different characteristics than the tephra from literature. MeR contents in Core 88s tephra were low, while tephra from literature showed high values (e.g. (Homoky et al., 2011) . This may be due to the fact that the tephra analyzed in literature is andesitic (Hembury et al., 2012; Homoky et al., 2011; Longman et al., 2019), while the tephra in this core is basaltic. Our data hints at a beneficial effect of tephra on OC preservation, but further study of basaltic tephra is required to fully understand it's impact and that differs from effects of other tephra facies. Currently, literature lacks data on varied tephra facies and their full potential in OC preservation. To date, only a single detailed study detailing tephra-OC interactions exists (Longman et al., 2021), with most conclusions drawn from studies in which tephra-OC interactions were analyzed tangentially (see (Longman et al., 2019). What is clear from comparison of our data with previous work is that the relationship between tephra deposition and OC preservation is non-linear.

5. Conclusions

In this study, we analyzed the composition of selected trace metals, organic carbon and reactive metals in a core recovered from the Aegir Ridge near Iceland, to determine if the Storegga Slide and tephra influenced organic carbon preservation within the sediments.

A large tephra layer in combination with the Storegga Slide appears to have caused reducing conditions to some degree in the sediments in between, with results appearing to suggest the original composition of the tephra is important in this process. Reactive metal phase (MeR) concentrations are lower in the tephra layer than in sediment layers, but this may be a function of high lithogenic background FeR concentrations in the sediment layers rather than low FeR in the tephra. A sediment layer found between the tephra layer and the Storegga Slide appears to have been strongly influenced by its location between these two events. The layer shows the highest amount of organic carbon preservation in the analyzed core-part, most likely due to the oxygen depleted tephra layer below and the sudden influx of sediment, that may have reduced the ability of seawater oxygen to percolate into the sediments below, caused by the Storegga Slide. Here, reduced oxidant exposure seems to have a stronger influence on the OC preservation process than the complexation with MeR. These topmost sediment samples above the Storegga Slide also show that favorable conditions for OC preservation do not always lead to enhanced OC preservation, as these samples display the lowest OC concentrations of the analyzed part of Core 88, despite geochemical data suggesting conditions favorable for OC preservation. Our findings indicate, that tephra and turbidites can positively influence OC preservation. While research on turbidite facies and their control on OM types and preservation is expanding, understanding on the influences of tephra facies and the resulting differences in preservation mechanisms, let alone the combination of turbidites and tephra, is sparse. To understand the degree to which these can influence OC preservation processes and the global carbon cycle, in-depth studies of the geochemical composition of tephra facies and of regions with mixtures of turbidites and tephra need to be done.

Declaration of Competing Interest

The authors declare that they have no known competing financial interests or personal relationships that could have appeared to influence the work reported in this paper.

Data availability

All data related to this article may be found in the supplementary information.

Appendix A. Supplementary data

Supplementary data to this article can be found online at https://doi.org/10.1016/j.margeo.2023.107120.

References

Achterberg, E.P., Moore, C.M., Henson, S.A., Steigenberger, S., Stohl, A., Eckhardt, S., Avendano, L.C., Cassidy, M., Hembury, D., Klar, J.K., 2013. Natural iron fertilization by the Eyjafjallajökull volcanic eruption. Geophys. Res. Lett. 40 (5), 921–926.

Adelson, J., Helz, G., Miller, C., 2001. Reconstructing the rise of recent coastal anoxia; molybdenum in Chesapeake Bay sediments. Geochim. Cosmochim. Acta 65 (2), 237–252.

Aguiar, W., Meissner, K.J., Montenegro, A., Prado, L., Wainer, I., Carlson, A.E., Mata, M. M., 2021. Magnitude of the 8.2 ka event freshwater forcing based on stable isotope modelling and comparison to future Greenland melting. Sci. Rep. 11 (1), 1–10.

Algeo, T.J., Li, C., 2020. Redox classification and calibration of redox thresholds in sedimentary systems. Geochim. Cosmochim. Acta 287, 8–26.

Algeo, T.J., Liu, J., 2020. A re-assessment of elemental proxies for paleoredox analysis. Chem. Geol. 540, 119549.

Aller, R.C., 1994. Bioturbation and remineralization of sedimentary organic matter: effects of redox oscillation. Chem. Geol. 114 (3–4), 331–345.

Anderson, R.F., 1982. Concentration, vertical flux, and remineralization of particulate uranium in seawater. Geochim. Cosmochim. Acta 46 (7), 1293–1299.

Barber, D.C., Dyke, A., Hillaire-Marcel, C., Jennings, A.E., Andrews, J.T., Kerwin, M.W., Bilodeau, G., McNeely, R., Southon, J., Morehead, M.D., 1999. Forcing of the cold event of 8,200 years ago by catastrophic drainage of Laurentide lakes. Nature 400 (6742), 344–348.

Barber, A., Brandes, J., Leri, A., Lalonde, K., Balind, K., Wirick, S., Wang, J., Gélinas, Y., 2017. Preservation of organic matter in marine sediments by inner-sphere interactions with reactive iron. Sci. Rep. 7 (1), 366. https://doi.org/10.1038/s41598-017-00494-0.

Basile-Doelsch, I., Amundson, R., Stone, W., Borschneck, D., Bottero, J.-Y., Moustier, S., Masin, F., Colin, F., 2007. Mineral control of carbon pools in a volcanic soil horizon. Geoderma 137 (3–4), 477–489.

Biscara, L., Mulder, T., Martinez, P., Baudin, F., Etcheber, H., Jouanneau, J.-M., Garlan, T., 2011. Transport of terrestrial organic matter in the Ogooué deep sea turbidite system (Gabon). Mar. Pet. Geol. 28 (5), 1061–1072.

Bondevik, S., Mangerud, J., Dawson, S., Dawson, A., Lohne, Ø., 2005. Evidence for three North Sea tsunamis at the Shetland Islands between 8000 and 1500 years ago. Quat. Sci. Rev. 24 (14–15), 1757–1775.

Breit, G.N., Wanty, R.B., 1991. Vanadium accumulation in carbonaceous rocks: a review of geochemical controls during deposition and diagenesis. Chem. Geol. 91 (2), 83–97.

Brothers, D.S., Luttrell, K.M., Chaytor, J.D., 2013. Sea-level–induced seismicity and submarine landslide occurrence. Geology 41 (9), 979–982.

Browning, T.J., Stone, K., Bouman, H.A., Mather, T.A., Pyle, D.M., Moore, C.M., Martinez-Vicente, V., 2015. Volcanic ash supply to the surface ocean—remote sensing of biological responses and their wider biogeochemical significance. Front. Mar. Sci. 2, 14.

Brumsack, H.-J., 1989. Geochemistry of recent TOC-rich sediments from the Gulf of California and the Black Sea. Geol. Rundsch. 78 (3), 851–882.

Bryn, P., Berg, K., Forsberg, C.F., Solheim, A., Kvalstad, T.J., 2005. Explaining the Storegga slide. Mar. Pet. Geol. 22 (1–2), 11–19.

Burdige, D.J., 1993. The biogeochemistry of manganese and iron reduction in marine sediments. Earth Sci. Rev. 35 (3), 249–284.

Burdige, D.J., 2005. Burial of terrestrial organic matter in marine sediments: a re-assessment. Glob. Biogeochem. Cycles 19 (4).

Burdige, D.J., 2007. Preservation of organic matter in marine sediments: controls, mechanisms, and an imbalance in sediment organic carbon budgets? Chem. Rev. 107 (2), 467–485.

Cai, G.-Q., Qiu, Y., Peng, X.-C., Zhang, Y.-L., Zhong, H.-X., 2010. Geochemical Characteristics of Barium in Surface Sediments fromthe Southwestern Area of South China Sea. Geoscience 24 (3), 560.

Calvert, S., Pedersen, T., 1993. Geochemistry of recent oxic and anoxic marine sediments: implications for the geological record. Mar. Geol. 113 (1–2), 67–88.

Cole, J.J., Hararuk, O., Solomon, C.T., 2021. The carbon cycle: With a brief introduction to global biogeochemistry. In: Fundamentals of Ecosystem Science. Elsevier, pp. 131–160.

Costa, K.M., Anderson, R.F., McManus, J.F., Winckler, G., Middleton, J.L., Langmuir, C. H., 2018. Trace element (Mn, Zn, Ni, V) and authigenic uranium (aU) geochemistry reveal sedimentary redox history on the Juan de Fuca Ridge, North Pacific Ocean. Geochim. Cosmochim. Acta 236, 79–98. https://doi.org/10.1016/j.gca.2018.02.016.

Crusius, J., Thomson, J., 2000. Comparative behavior of authigenic Re, U, and Mo during reoxidation and subsequent long-term burial in marine sediments. Geochim. Cosmochim. Acta 64 (13), 2233–2242.

Crusius, J., Calvert, S., Pedersen, T., Sage, D., 1996. Rhenium and molybdenum enrichments in sediments as indicators of oxic, suboxic and sulfidic conditions of deposition. Earth Planet. Sci. Lett. 145 (1–4), 65–78.
Dawson, A., Bondevik, S., Teller, J., 2011. Relative timing of the Storegga submarine slide, methane release, and climate change during the 8.2 ka cold event. The Holocene 21 (7), 1167–1171.
Dean, W.E., Gardner, J., 1982. Origin and geochemistry of redox cycles of jurassic to eocene age, Cape Verde Basin (DSDP Site 367), Continental Margin of North-West Africa. In: Nature and origin of Cretaceous carbon-rich facies. Symposium.
DeVries, T., Primeau, F., Deutsch, C., 2012. The sequestration efficiency of the biological pump. Geophys. Res. Lett. 39 (13).
Duggen, S., Olgun, N., Croot, P., Hoffmann, L.J., Dietze, H., Delmelle, P., Teschner, C., 2010. The role of airborne volcanic ash for the surface ocean biogeochemical iron-cycle: a review. Biogeosciences (BG) 7 (3), 827–844.
Dunne, J.P., Sarmiento, J.L., Gnanadesikan, A., 2007. A synthesis of global particle export from the surface ocean and cycling through the ocean interior and on the seafloor. Glob. Biogeochem. Cycles 21 (4).
Dymond, J., Suess, E., Lyle, M., 1992. Barium in deep-sea sediment: a geochemical proxy for paleoproductivity. Paleoceanography 7 (2), 163–181.
Evans, D., Harrison, Z., Shannon, P., Laberg, J., Nielsen, T., Ayers, S., Holmes, R., Hoult, R., Lindberg, B., Haflidason, H., 2005. Palaeoslides and other mass failures of Pliocene to Pleistocene age along the Atlantic continental margin of NW Europe. Mar. Pet. Geol. 22 (9–10), 1131–1148.
Falkowski, P.G., Barber, R.T., Smetacek, V., 1998. Biogeochemical controls and feedbacks on ocean primary production. Science 281 (5374), 200–206.
Falkowski, P., Scholes, R., Boyle, E., Canadell, J., Canfield, D., Elser, J., Gruber, N., Hibbard, K., Högberg, P., Linder, S., 2000. The global carbon cycle: a test of our knowledge of earth as a system. Science 290 (5490), 291–296.
Faust, J.C., Tessin, A., Fisher, B.J., Zindorf, M., Papadaki, S., Hendry, K.R., Doyle, K.A., März, C., 2021. Millennial scale persistence of organic carbon bound to iron in Arctic marine sediments. Nat. Commun. 12 (1), 1–9.
Froelich, P.N., Klinkhammer, G., Bender, M.L., Luedtke, N., Heath, G.R., Cullen, D., Dauphin, P., Hammond, D., Hartman, B., Maynard, V., 1979. Early oxidation of organic matter in pelagic sediments of the eastern equatorial Atlantic: suboxic diagenesis. Geochim. Cosmochim. Acta 43 (7), 1075–1090.
Govindaraju, K., 1994. 1994 compilation of working values and sample description for 383 geostandards. Geostand. Newslett. 18, 1–158.
Haeckel, M., van Beusekom, J., Wiesner, M.G., König, I., 2001. The impact of the 1991 Mount Pinatubo tephra fallout on the geochemical environment of the deep-sea sediments in the South China Sea. Earth Planet. Sci. Lett. 193 (1–2), 151–166.
Haflidason, H., Lien, R., Sejrup, H.P., Forsberg, C.F., Bryn, P., 2005. The dating and morphometry of the Storegga Slide. Mar. Pet. Geol. 22 (1–2), 123–136.
Hage, S., Galy, V., Cartigny, M., Acikalin, S., Clare, M., Gröcke, D., Hilton, R., Hunt, J., Lintern, D., McGhee, C., 2020. Efficient preservation of young terrestrial organic carbon in sandy turbidity-current deposits. Geology 48 (9), 882–887.
Hage, S., Romans, B.W., Peploe, T.G., Poyatos-Moré, M., Haeri Ardakani, O., Bell, D., Englert, R.G., Kaempfe-Droguett, S.A., Nesbit, P.R., Sherstan, G., 2022. High rates of organic carbon burial in submarine deltas maintained on geological timescales. Nat. Geosci. 1–6.
Hartnett, H.E., Keil, R.G., Hedges, J.I., Devol, A.H., 1998. Influence of oxygen exposure time on organic carbon preservation in continental margin sediments. Nature 391 (6667), 572–575.
Hembury, D., Palmer, M., Fones, G., Mills, R., Marsh, R., Jones, M., 2012. Uptake of dissolved oxygen during marine diagenesis of fresh volcanic material. Geochim. Cosmochim. Acta 84, 353–368.
Henrichs, S.M., 1992. Early diagenesis of organic matter in marine sediments: progress and perplexity. Mar. Chem. 39 (1–3), 119–149.
Hijma, M.P., Cohen, K.M., 2010. Timing and magnitude of the sea-level jump preluding the 8200 yr event. Geology 38 (3), 275–278.
Hjelstuen, B.O., Andreassen, E.V., 2015. North Atlantic Ocean deep-water processes and depositional environments: a study of the Cenozoic Norway Basin. Mar. Pet. Geol. 59, 429–441.
Hjelstuen, B.O., Sejrup, H.P., Haflidason, H., Nygård, A., Ceramicola, S., Bryn, P., 2005. Late Cenozoic glacial history and evolution of the Storegga Slide area and adjacent slide flank regions, Norwegian continental margin. In: Ormen Lange–An Integrated Study for Safe Field Development in the Storegga Submarine Area. Elsevier, pp. 57–69.
Homoky, W., Hembury, D., Hepburn, L., Mills, R., Statham, P., Fones, G., Palmer, M., 2011. Iron and manganese diagenesis in deep sea volcanogenic sediments and the origins of pore water colloids. Geochim. Cosmochim. Acta 75 (17), 5032–5048.
Horwell, C., Fenoglio, I., Fubini, B., 2007. Iron-induced hydroxyl radical generation from basaltic volcanic ash. Earth Planet. Sci. Lett. 261 (3–4), 662–669.
Hoshyaripour, G., Hort, M., Langmann, B., Delmelle, P., 2014. Volcanic controls on ash iron solubility: New insights from high-temperature gas–ash interaction modeling. J. Volcanol. Geotherm. Res. 286, 67–77.
Huc, A., Bertrand, P., Stow, D.V., Gayet, J., Vandenbroucke, M., 2001. Organic sedimentation in deep offshore settings: the Quaternary sediments approach. Mar. Pet. Geol. 18 (4), 513–517.
Huerta-Diaz, M.A., Morse, J.W., 1992. Pyritization of trace metals in anoxic marine sediments. Geochim. Cosmochim. Acta 56 (7), 2681–2702.
Hussain, A., Haughton, P.D., Shannon, P.M., Morris, E.A., Pierce, C.S., Omma, J.E., 2021. Mud-forced turbulence dampening facilitates rapid burial and enhanced preservation of terrestrial organic matter in deep-sea environments. Mar. Pet. Geol. 130, 105101.
Jochum, K.P., Weis, U., Schwager, B., Stoll, B., Wilson, S.A., Haug, G.H., Andreae, M.O., Enzweiler, J., 2016. Reference values following ISO guidelines for frequently requested rock reference materials. Geostand. Geoanal. Res. 40 (3), 333–350.
Johnson, K.S., Berelson, W.M., Coale, K.H., Coley, T.L., Elrod, V.A., Fairey, W.R., Iams, H.D., Kilgore, T.E., Nowicki, J.L., 1992. Manganese flux from continental margin sediments in a transect through the oxygen minimum. Science 257 (5074), 1242–1245.
Johnson, K., Purvis, G., Lopez-Capel, E., Peacock, C., Gray, N., Wagner, T., März, C., Bowen, L., Ojeda, J., Finlay, N., 2015. Towards a mechanistic understanding of carbon stabilization in manganese oxides. Nat. Commun. 6 (1), 1–11.
Kostka, J.E., Luther III, G.W., 1994. Partitioning and speciation of solid phase iron in saltmarsh sediments. Geochim. Cosmochim. Acta 58 (7), 1701–1710.
Kvalstad, T.J., Andresen, L., Forsberg, C.F., Berg, K., Bryn, P., Wangen, M., 2005. The Storegga slide: evaluation of triggering sources and slide mechanics. In: Ormen Lange–An Integrated Study for Safe Field Development in the Storegga Submarine Area. Elsevier, pp. 245–256.
Lalonde, K., Mucci, A., Ouellet, A., Gélinas, Y., 2012. Preservation of organic matter in sediments promoted by iron. Nature 483 (7388), 198–200. https://doi.org/10.1038/nature10855.
Little, S.H., Vance, D., Lyons, T.W., McManus, J., 2015. Controls on trace metal authigenic enrichment in reducing sediments: insights from modern oxygen-deficient settings. Am. J. Sci. 315 (2), 77–119.
Longman, J., Palmer, M.R., Gernon, T.M., Manners, H.R., 2019. The role of tephra in enhancing organic carbon preservation in marine sediments. Earth Sci. Rev. 192, 480–490. https://doi.org/10.1016/j.earscirev.2019.03.018.
Longman, J., Palmer, M.R., Gernon, T.M., 2020. Viability of greenhouse gas removal via artificial addition of volcanic ash to the ocean. Anthropocene 32, 100264.
Longman, J., Gernon, T.M., Palmer, M.R., Manners, H.R., 2021. Tephra deposition and bonding with reactive oxides enhances burial of organic carbon in the Bering Sea. Glob. Biogeochem. Cycles 35 (11) e2021GB007140.
Longman, J., Faust, J., Bryce, C., Homoky, W.B., März, C., 2022a. Organic Carbon Burial with Reactive iron across Global Environments.
Longman, J., Palmer, M.R., Gernon, T.M., Manners, H.R., Jones, M.T., 2022b. Subaerial volcanism is a potentially major contributor to oceanic iron and manganese cycles. Communicat. Earth & Environ. 3 (1), 1–8.
Lu, Y., Jiang, S., Lu, Y., Xu, S., Shu, Y., Wang, Y., 2019. Productivity or preservation? The factors controlling the organic matter accumulation in the late Katian through Hirnantian Wufeng organic-rich shale, South China. Mar. Pet. Geol. 109, 22–35.
Maters, E.C., Delmelle, P., Gunnlaugsson, H.P., 2017. Controls on iron mobilisation from volcanic ash at low pH: Insights from dissolution experiments and Mössbauer spectroscopy. Chem. Geol. 449, 73–81.
McLennan, S.M., Taylor, S., Kröner, A., 1983. Geochemical evolution of Archean shales from South Africa. I. the Swaziland and Pongola Supergroups. Precambrian Res. 22 (1–2), 93–124.
Mehra, O., Jackson, M., 2013. Iron oxide removal from soils and clays by a dithionite–citrate system buffered with sodium bicarbonate. In: Clays and Clay Minerals. Elsevier, pp. 317–327.
Meyers, P.A., Silliman, J.E., Shaw, T.J., 1996. Effects of turbidity flows on organic matter accumulation, sulfate reduction, and methane generation in deep-sea sediments on the Iberia Abyssal Plain. Org. Geochem. 25 (1–2), 69–78.
Moore, C.M., Mills, M.M., Arrigo, K.R., Berman-Frank, I., Bopp, L., Boyd, P.W., Galbraith, E.D., Geider, R.J., Guieu, C., Jaccard, S.L., Jickells, T.D., La Roche, J., Lenton, T.M., Mahowald, N.M., Marañón, E., Marinov, I., Moore, J.K., Nakatsuka, T., Oschlies, A., Ulloa, O., 2013. Processes and patterns of oceanic nutrient limitation. Nat. Geosci. 6 (9), 701–710. https://doi.org/10.1038/ngeo1765.
Morford, J.L., Emerson, S., 1999. The geochemistry of redox sensitive trace metals in sediments. Geochim. Cosmochim. Acta 63 (11−12), 1735–1750.
Morford, J.L., Martin, W.R., Carney, C.M., 2009. Uranium diagenesis in sediments underlying bottom waters with high oxygen content. Geochim. Cosmochim. Acta 73 (10), 2920–2937.
Mosar, J., Eide, E.A., Osmundsen, P.T., Sommaruga, A., Torsvik, T.H., 2002. Greenland–Norway separation: a geodynamic model for the North Atlantic. Nor. J. Geol. 82, 282.
Olgun, N., Duggen, S., Croot, P.L., Delmelle, P., Dietze, H., Schacht, U., Óskarsson, N., Siebe, C., Auer, A., Garbe-Schönberg, D., 2011. Surface Ocean iron fertilization: the role of airborne volcanic ash from subduction zone and hot spot volcanoes and related iron fluxes into the Pacific Ocean. Glob. Biogeochem. Cycles 25 (4).
Osman, M.B., Tierney, J.E., Zhu, J., Tardif, R., Hakim, G.J., King, J., Poulsen, C.J., 2021. Globally resolved surface temperatures since the last Glacial Maximum. Nature 599 (7884), 239–244.
Passow, U., Carlson, C.A., 2012. The biological pump in a high CO2 world. Mar. Ecol. Prog. Ser. 470, 249–271.
Paull, C.K., Ussler III, W., Holbrook, W.S., Hill, T.M., Haflidason, H., Winters, W., Lorenson, T., Aiello, I., Johnson, J.E., Lundsten, E., 2010. The tail of the Storegga Slide: insights from the geochemistry and sedimentology of the Norwegian Basin deposits. Sedimentology 57 (6), 1409–1429.
Pierau, R., Henrich, R., Preiß-Daimler, I., Krastel, S., Geersen, J., 2011. Sediment transport and turbidite architecture in the submarine Dakar Canyon off Senegal, NW-Afric. J. Afr. Earth Sci. 60 (3), 196–208.
Pohl, A., Donnadieu, Y., Le Hir, G., Ferreira, D., 2017. The climatic significance of late Ordovician-early Silurian black shales. Paleoceanography 32 (4), 397–423.
Roy, M., McManus, J., Goñi, M.A., Chase, Z., Borgeld, J.C., Wheatcroft, R.A., Muratli, J. M., Megowan, M.R., Mix, A., 2013. Reactive iron and manganese distributions in seabed sediments near small mountainous rivers off Oregon and California (USA). Cont. Shelf Res. 54, 67–79. https://doi.org/10.1016/j.csr.2012.12.012.

Rullkötter, J., Cornford, C., Welte, D.H., 1982. Geochemistry and petrography of organic matter in Northwest African continental margin sediments: quantity, provenance, depositional environment and temperature history. In: Geology of the Northwest African Continental Margin. Springer, pp. 686–703.
Saller, A., Lin, R., Dunham, J., 2006. Leaves in turbidite sands: the main source of oil and gas in the deep-water Kutei Basin, Indonesia. AAPG Bull. 90 (10), 1585–1608.
Schoepfer, S.D., Shen, J., Wei, H., Tyson, R.V., Ingall, E., Algeo, T.J., 2015. Total organic carbon, organic phosphorus, and biogenic barium fluxes as proxies for paleomarine productivity. Earth Sci. Rev. 149, 23–52.
Scholz, F., Hensen, C., Noffke, A., Rohde, A., Liebetrau, V., Wallmann, K., 2011. Early diagenesis of redox-sensitive trace metals in the Peru upwelling area – response to ENSO-related oxygen fluctuations in the water column. Geochim. Cosmochim. Acta 75 (22), 7257–7276. https://doi.org/10.1016/j.gca.2011.08.007.
Shanmugam, G., 2002. Ten turbidite myths. Earth Sci. Rev. 58 (3–4), 311–341.
Smith, D.E., Shi, S., Cullingford, R.A., Dawson, A.G., Dawson, S., Firth, C.R., Foster, I.D., Fretwell, P.T., Haggart, B.A., Holloway, L.K., 2004. The holocene storegga slide tsunami in the United Kingdom. Quat. Sci. Rev. 23 (23–24), 2291–2321.
Smith, R.W., Bianchi, T.S., Allison, M., Savage, C., Galy, V., 2015. High rates of organic carbon burial in fjord sediments globally. Nat. Geosci. 8 (6), 450–453.
Tanhua, T., Bates, N.R., Körtzinger, A., 2013. The marine carbon cycle and ocean carbon inventories. In: International Geophysics, vol. 103. Elsevier, pp. 787–815.
Thomson, J., Higgs, N., Croudace, I., Colley, S., Hydes, D., 1993. Redox zonation of elements at an oxic/post-oxic boundary in deep-sea sediments. Geochim. Cosmochim. Acta 57 (3), 579–595.
Thomson, J., Jarvis, I., Green, D.R., Green, D.A., Clayton, T., 1998. Mobility and immobility of redox-sensitive elements in deep-sea turbidites during shallow burial. Geochim. Cosmochim. Acta 62 (4), 643–656.
Törnqvist, T.E., Bick, S.J., González, J.L., van der Borg, K., de Jong, A.F., 2004. Tracking the sea-level signature of the 8.2 ka cooling event: New constraints from the Mississippi Delta. Geophys. Res. Lett. 31 (23).
Tribovillard, N., Algeo, T.J., Lyons, T., Riboulleau, A., 2006. Trace metals as paleoredox and paleoproductivity proxies: an update. Chem. Geol. 232 (1–2), 12–32.
Von der Heyden, B., Roychoudhury, A., Mtshali, T., Tyliszczak, T., Myneni, S.C.B., 2012. Chemically and geographically distinct solid-phase iron pools in the Southern Ocean. Science 338 (6111), 1199–1201.
Watson, A.J., Schuster, U., Shutler, J.D., Holding, T., Ashton, I.G., Landschützer, P., Woolf, D.K., Goddijn-Murphy, L., 2020. Revised estimates of ocean-atmosphere CO2 flux are consistent with ocean carbon inventory. Nat. Commun. 11 (1), 1–6.
Watts, C., 2019. Submarine Mega-Slides from the Norwegian Continental Margin and their Relationship to Periods of Climatic Change. University of Southampton.
Weimer, P., Link, M.H., 1991. Global petroleum occurrences in submarine fans and turbidite systems. In: Seismic Facies and Sedimentary Processes of Submarine Fans and Turbidite Systems. Springer, pp. 9–67.